

# One Sample is Enough to Make Conformal Prediction Robust

Soroush H. Zargarbashi<sup>1</sup> Mohammad Sadegh Akhondzadeh<sup>2</sup> Aleksandar Bojchevski<sup>2</sup>

<sup>1</sup> CISPA Helmholtz Center for Information Security, <sup>2</sup> University of Cologne  
[zargarbashi, akhondzadeh, bojchevski]@cs.uni-koeln.de

## Abstract

Given any model, conformal prediction (CP) returns prediction *sets* guaranteed to include the true label with high adjustable probability. Robust CP (RCP) extends this to inputs with worst-case noise. A well-established approach is to use randomized smoothing for RCP since it is applicable to any black-box model and provides smaller sets compared to deterministic methods. However, current smoothing-based RCP requires many model forward passes per each input which is computationally expensive. We show that conformal prediction attains some robustness even with a forward pass on a *single* randomly perturbed input. Using any binary certificate we propose a single sample robust CP (RCP1). Our approach returns robust sets with smaller average set size compared to SOTA methods which use many (e.g.  $\sim 100$ ) passes per input. Our key insight is to certify the conformal prediction procedure itself rather than individual scores. Our approach is agnostic to the setup (classification and regression). We further extend our approach to smoothing-based robust conformal risk control.

## 1 Introduction

Modern neural networks return uncalibrated probability estimates [13]. Other uncertainty quantification methods (e.g. Bayesian and ensemble models, Monte-Carlo dropout, etc.) are computationally expensive. Furthermore, they do not usually provide formal statistical guarantees. Alternatively, conformal prediction (CP) is a statistical post-processing method returning prediction *sets* with a distribution-free and model agnostic coverage guarantee. To apply CP, we need a score function capturing the agreement between  $x$ , and  $y$  (e.g. softmax). We compute a conformal threshold over a holdout set of calibration points, and for the future test points, we form the set as all labels with scores exceeding that threshold.<sup>1</sup> These sets are guaranteed to include (to cover) the true label with adjustable  $1 - \alpha$  probability [2]. This guarantee breaks with a small natural or adversarial noise added to the test points – the empirical coverage drastically decreases even when an imperceptible perturbation is introduced (see Fig. 1-left). Detailed descriptions for figures are in § B.

Robust CP (RCP) extends this guarantee to worst case bounded perturbations, the perturbed input  $\tilde{x}$  is covered with the same guarantee as the clean  $x$  up to a given radius  $r$  (e.g.  $\|\tilde{x} - x\|_2 \leq r$ ). Previous RCP approaches find the minimum or maximum possible score within the perturbation ball, and use that bound as the score instead [11, 14, 24, 23]. Randomized smoothing is extensively used for RCP since for nearby  $x$  and  $\tilde{x}$  the distribution of their smooth scores has a large overlap. For example, consider the smoothing as augmenting the input  $x$  with isotropic Gaussian noise  $\epsilon$ , and the smooth score as the mean of the outputs distribution  $\mathbb{E}_\epsilon[s(x + \epsilon, y)]$ . We can find a lower bound for this score, and use it to change the threshold with which we accept each label under perturbation.

<sup>1</sup>Many works define CP via a non-conformity (disagreement) score. The setups are equivalent with a change in the score’s sign. Our robustness results are invariant to this definition.

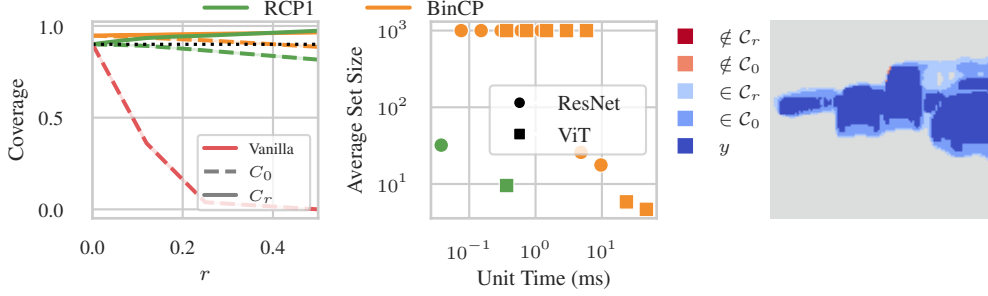


Figure 1: [Left] Coverage of vanilla CP, our robust RCP1, and the SOTA BinCP sets under attack (§B).  $C_r$  denotes sets that are guaranteed robust up to a perturbation of radius  $r$ . Even the  $C_0$  sets which have no guarantees are more robust than vanilla due to randomized smoothing. [Middle] The average time to compute, and the average size of prediction sets with ResNet and ViT models on the ImageNet dataset; both axis are log-scaled and pareto-optimal points are at the lower-left. RCP1 is more efficient. Both plots with  $\sigma = 0.5$ . [Right] Smoothing-based robust conformal risk control. We show the coverage and miscoverage of the RCP1 mask for the class "car" in the segmentation task.

An important drawback of these methods is their computational overhead. This is due to the design of the score function (e.g. mean of the smooth score distribution) that has to be estimated with Monte-Carlo sampling. By reducing the sample rate used for this estimation, the average size of the prediction sets quickly increases since the confidence intervals expand. An efficient alternative is to use neural network verifiers [14], however, they are limited to simpler models, and small radii. The question is: Can we design smoothing-based RCP without introducing computational overhead?

Interestingly, we show the vanilla CP combined with noise-augmented inference already has robust behavior (see Fig. 1-left). This allows us to directly apply robustness certificates on CP’s guarantee. Compared to mean, CDF, or quantile-based scores used in other RCPs, we do not need to estimate any statistics via sampling. We define RCP1 (robust conformal prediction with one sample) that returns sets with a similar size, and guarantee as the SOTA methods that require many forward passes per input. For instance, RCP1 returns sets similar to BinCP [24] which needs at least 70 to 110 samples per input. By nullifying the need for sampling we can use even larger models and hence return even smaller sets (see Fig. 1-middle). Importantly, we do not compete with the SOTA when the number of samples (and compute) is unlimited, instead, we propose a compute-friendly alternative that produces small prediction sets that can also work in settings infeasible for the other smoothing-based RCP methods.

RCP1 is easy to implement, agnostic to the distribution of inputs and scores: use the smoothing scheme to augment each datapoint *once*, and run the conformal calibration similar to the vanilla setup but instead with a conservative  $1 - \alpha'$  nominal coverage. We choose  $1 - \alpha'$  such that our certified lower bound remains above  $1 - \alpha$  (see § 3). RCP1 is compatible with any black-box model and binary certificate. For instance, we were able to extend Yang et al. [22]’s classification certificates to obtain robust CP for various smoothing schemes and threat models (see § 3.1). Similarly, with small changes the same process can be used to define a smoothing-based conformal risk control (see Fig. 1-right). Interestingly, since the guarantee is over the coverage probability (and not the scores), one can use a *binary* certificates to attain smoothing-based robust prediction intervals for robust conformal regression as well.

## 2 Background

CP requires a holdout set of labeled calibration points  $\mathcal{D}_{\text{cal}} = \{\mathbf{x}_i, y_i\}_{i=1}^n$  that is exchangeable with the future test point  $\mathbf{x}_{n+1}$ . From the model’s output, we define a score function  $s : \mathcal{X} \times \mathcal{Y} \rightarrow \mathbb{R}$  where it quantifies the agreement between  $\mathbf{x}$ , and  $y$ , for example softmax, see § C for other scores. Vovk et al. [19] show that under exchangeability (vanilla setup) the set  $\mathcal{C}_0(\mathbf{x}_{n+1}) = \{y : s(\mathbf{x}_{n+1}, y) \geq q\}$  for  $q = \mathbb{Q}(\alpha; \{s(\mathbf{x}_i, y_i) : (\mathbf{x}_i, y_i) \in \mathcal{D}_{\text{cal}}\})$  contains the true label  $y_{n+1}$  at least with  $1 - \alpha$  probability.

$$\Pr_{\mathcal{D}_+}[y_{n+1} \in \mathcal{C}_0(\mathbf{x}_{n+1})] = \Pr_{\mathcal{D}_+}[s(\mathbf{x}_{n+1}, y_{n+1}) \geq q] \geq 1 - \alpha \quad (1)$$

Here  $\mathcal{D}_+ = \mathcal{D}_{\text{cal}} \cup \{(\mathbf{x}_{n+1}, y_{n+1})\}$ , and  $\mathbb{Q}(\alpha; \mathcal{A})$  is the  $\alpha \cdot (1 - \frac{1}{n+1})$  quantile of the set  $\mathcal{A}$ . The coverage guarantee is distribution-free and agnostic to the model, and the score function. Better score

functions (or models) reflect in other properties like the prediction set size; a.k.a efficiency. Our approach is also agnostic to the choice of the score function (bounded or unbounded).

**Threat model.** With (worst-case) perturbations, the exchangeability breaks and the empirical coverage drastically decreases from the guaranteed level (see Fig. 1-left). The adversary aims to decrease the empirical coverage below the guaranteed  $1 - \alpha$  by adding an imperceptible noise to the test points (evasion). The set of all possible perturbations is defined as a ball  $\mathcal{B} : \mathcal{X} \rightarrow 2^{\mathcal{X}}$  around the clean input. The inverted ball  $\mathcal{B}^{-1}$  is defined as the smallest set that  $\forall \tilde{x} \in \mathcal{B}(x) \Rightarrow x \in \mathcal{B}^{-1}(\tilde{x})$ , the smallest set which for any perturbation it includes the clean input. For images, a common threat model is  $\ell_2$ -norm:  $\mathcal{B}_r(x) = \{\tilde{x} : \|\tilde{x} - x\|_2 \leq r\}$  where  $r$  is the radius of the perturbation. For symmetric balls like  $\ell_2$  we have  $\mathcal{B} = \mathcal{B}^{-1}$ . This does not hold in general, e.g. for the sparse ball [4].

**Robust Conformal Prediction (RCP).** Robust CP extends the guarantee in Eq. 1 to the worst case noise. For  $\mathcal{B}$ , it defines robust (conservative) prediction set  $\mathcal{C}_{\mathcal{B}}$  satisfying the following

$$\Pr_{\mathcal{D}_{\text{cal}}, \mathbf{x}_{n+1} \sim \mathcal{D}}[y_{n+1} \in \mathcal{C}_{\mathcal{B}}(\tilde{\mathbf{x}}_{n+1}), \forall \tilde{\mathbf{x}}_{n+1} \in \mathcal{B}(\mathbf{x}_{n+1})] \geq 1 - \alpha \quad (2)$$

Zargarbashi et al. [24] show that if the score is bounded within  $\mathcal{B}$ , i.e.  $\forall \tilde{\mathbf{x}}_{n+1} \in \mathcal{B}(\mathbf{x}_{n+1}), c^{\downarrow}[s(\cdot, y_{n+1}), \mathbf{x}_{n+1}; \mathcal{B}] \leq s(\tilde{\mathbf{x}}_{n+1}, y_{n+1}) \leq c^{\uparrow}[s(\cdot, y_{n+1}), \mathbf{x}_{n+1}; \mathcal{B}]$ , the conservative sets defined either as  $\mathcal{C}_{\mathcal{B}}(\mathbf{x}_{n+1}) = \{y : c^{\uparrow}[s(\cdot, y), \mathbf{x}_{n+1}; \mathcal{B}^{-1}] \geq q\}$  (test-time RCP), or similarly,  $\mathcal{C}_{\mathcal{B}}(\mathbf{x}_{n+1}) = \{y : c^{\uparrow}[s(\cdot, y), \mathbf{x}_{n+1}; \mathcal{B}^{-1}] \geq \bar{q}\}$  for  $\bar{q} = \mathbb{Q}(\alpha; \{c^{\downarrow}[s(\cdot, y_i), \mathbf{x}_i; \mathcal{B}] : (\mathbf{x}_i, y_i) \in \mathcal{D}_{\text{cal}}\})$  (calibration-time RCP) attain  $1 - \alpha$  robust coverage. Here  $c^{\downarrow}[f, x, \mathcal{B}]$  is the certified lower bound for the function  $f$  over any point within  $\mathcal{B}(x)$ ;  $c^{\uparrow}$  is similarly the upper bound.

**Randomized smoothing.** One approach to compute these upper/lower bounds for any black-box model, or score is randomized smoothing. A smoothing scheme  $\xi : \mathcal{X} \rightarrow \mathcal{X}$  adds a random noise to the input – maps it to a random point close to it. A common smoothing for continuous data (e.g. images) is the Gaussian smoothing  $\xi(x) = x + \epsilon$  where  $\epsilon$  is an isotropic Gaussian noise  $\epsilon \sim \mathcal{N}(\mathbf{0}, \sigma \mathbf{I})$ . While our method works for any smoothing, for easier notation we further use  $x + \epsilon$  instead of  $\xi(x)$ .

For any score function  $s$ , the distribution of the smooth scores  $s(x + \epsilon, y)$  changes slowly. This enables us to compute tight bounds on the smooth statistics (mean, quantile, etc.) within  $\mathcal{B}$ , or  $\mathcal{B}^{-1}$ . RSCP [11, 21], and CAS [24] set the score function directly to the mean of the distribution. BinCP [23], uses the  $p$ -quantile instead. These statistics are often intractable to compute and therefore estimated using Monte-Carlo sampling, followed by a finite sample correction. RCP1 however nullifies the need to estimate these statistics. We discuss the related work further in § A.

### 3 RCP1: Robust CP with a Single Sample

Almost all smoothing RCP frameworks work through the following chain of arguments: (i) for the exchangeable  $\mathbf{x}_{n+1}$  conformal prediction covers the true label with  $1 - \alpha$  probability, (ii) if the clean  $\mathbf{x}_{n+1}$  was originally covered by (vanilla) CP, robust CP also covers  $\tilde{\mathbf{x}}_{n+1}$ , because if a score is above  $q$  it's upper bound is also above  $q$ . Thus, the vanilla set for  $\mathbf{x}_{n+1}$  is a subset of the robust set for  $\tilde{\mathbf{x}}_{n+1}$ . So we can conclude that robust CP has a coverage of *at least*  $1 - \alpha$ . Since Eq. 2 does not account for the inherent randomness of the CP itself, it is vague for random scores (like APS – see § C) as in that setup  $y_{n+1} \in \mathcal{C}(\mathbf{x}_{n+1})$  is not binary. Here, the adversary's goal is to decrease the coverage probability over internal randomness of the process. Therefore, we replace the argument (ii) by the following: “the perturbed  $\tilde{\mathbf{x}}_{n+1}$  has a higher probability to be in the robust prediction set compared to  $\mathbf{x}_{n+1}$  being in the vanilla set”. Formally, with  $\mathcal{C}_0$  as the vanilla and  $\mathcal{C}_r$  as the robust set for a ball  $\mathcal{B}_r$  of radius  $r$  we have  $\Pr[\min_{\tilde{\mathbf{x}}_{n+1} \in \mathcal{B}(\mathbf{x}_{n+1})} \Pr[y_{n+1} \in \mathcal{C}_r(\tilde{\mathbf{x}}_{n+1})]] \geq \Pr[y_{n+1} \in \mathcal{C}_0(\mathbf{x}_{n+1})] \geq 1 - \alpha$ .

**General worst-case guarantee.** Let  $Z_i : i \in [n+1]$  be  $n+1$  exchangeable random variables, where  $Z_i = (X_i, Y_i)$  for  $X_i \in \mathcal{X}$  (e.g.  $\mathcal{X} = \mathbb{R}^d$ ), and  $Y_i \in \mathcal{Y}$  (e.g.  $\mathcal{Y} = [K]$ ). We can think of  $(x_i, y_i)$ 's as realizations of these random variables. Let  $s : \mathcal{X} \times \mathcal{Y} \rightarrow \mathbb{R}$  be any measurable score function. Let  $E_i : i \in [n+1]$  be i.i.d. random variables from a distribution supported on  $\mathcal{X}$  (e.g.  $E_i \sim \mathcal{N}(\mathbf{0}, \sigma^2 \mathbf{I})$ ). We define  $\hat{S}_i = s(X_i, Y_i)$ , and  $S_i = s(X_i + E_i, Y_i)$ . Let  $\delta \in \mathcal{B}_r$  be any arbitrary perturbation up to radius  $r$ , we define  $\tilde{X}_{n+1} = X_{n+1} + \delta$ , and  $\tilde{S}_{n+1} = s(\tilde{X}_{n+1} + E_{n+1}, Y_{n+1})$  accordingly.

**Proposition 1.** Let  $q = \mathbb{Q}(\alpha; s(X_i + E_i, Y_i) : (X_i, Y_i) \in \mathcal{D}_{\text{cal}})$ . Given a certified lower bound  $c^{\downarrow}[\cdot, \mathcal{B}]$  as later defined in Eq. 4, for any perturbation  $\delta \in \mathcal{B}_r$  we have

$$\Pr_{\mathcal{D}_{\text{cal}} \cup \{(X_{n+1}, Y_{n+1})\}, \{E_i\}_{i=1}^{n+1}}[s(\tilde{X}_{n+1} + E_{n+1}, Y_{n+1}) \geq q] \geq c^{\downarrow}[1 - \alpha, \mathcal{B}]$$

*Proof.* Adding i.i.d. noise  $E_i$  is permutation equivariant, thus  $S_i$ 's and  $\hat{S}_i$ 's are exchangeable. Let  $\mathcal{E}_+ = \{E_i\}_{i=1}^{n+1}$  and  $\mathcal{D}_+ = \mathcal{D}_{\text{cal}} \cup Z_{n+1}$  for convenience. From Vovk et al. [19] we have  $\Pr[\hat{S}_{n+1} \geq q] \geq 1 - \alpha$  for  $q = \mathbb{Q}(\alpha; \{\hat{S}_i\}_{i=1}^n)$ , and similarly  $\Pr[S_{n+1} \geq q \mid \mathcal{E}_+] \geq 1 - \alpha$  where both probabilities are over  $\mathcal{D}_+$ .<sup>2</sup> Importantly, if we now marginalize out all the  $E_i$ 's we still have  $\Pr_{\mathcal{D}_+, \mathcal{E}_+}[S_{n+1} \geq q] \geq 1 - \alpha$ . We can now rewrite

$$\Pr_{\mathcal{D}_+, \mathcal{E}_+}[S_{n+1} \geq q] = \mathbb{E}_{\mathcal{D}_+, \{E_i\}_{i=1}^n} \left[ \Pr_{E_{n+1}}[S_{n+1} \geq q \mid \mathcal{D}_+, \{E_i\}_{i=1}^n] \right] = \mathbb{E}_{\mathcal{D}_+, \{E_i\}_{i=1}^n}[\beta_{n+1}] \geq 1 - \alpha$$

where we have defined  $\beta_{n+1} := \Pr_{E_{n+1}}[S_{n+1} \geq q \mid \mathcal{D}_+, \{E_i\}_{i=1}^n]$  which is only a probability over the last noise  $E_{n+1}$  for a fixed  $\mathcal{D}_+$  and  $\{E_i\}_{i=1}^n$ . We call  $\beta_{n+1}$  the clean instance-wise coverage. We can bound any smooth binary function with an existing certified lower bound  $c^\downarrow[\cdot, \mathcal{B}]$ . Formally,

$$\Pr_{E_{n+1}}[S_{n+1} \geq q \mid \mathcal{D}_+, \{E_i\}_{i=1}^n] = \beta_{n+1} \Rightarrow \Pr_{E_{n+1}}[\tilde{S}_{n+1} \geq q \mid \mathcal{D}_+, \{E_i\}_{i=1}^n] \geq c^\downarrow[\beta_{n+1}, \mathcal{B}] \quad (3)$$

Note that here both probabilities share the same  $\mathcal{D}_+$ , and  $\{E_i\}_{i=1}^n$  and both are over the random variable  $E_{n+1}$ . Later in Lemma 1, we show that the function  $c^\downarrow[\beta, \mathcal{B}]$  is convex and increasing in  $\beta$ . This helps us to bound the adversarial coverage guarantee as

$$\begin{aligned} \Pr[Y_{n+1} \in \mathcal{C}(\tilde{X}_{n+1})] &= \Pr[\tilde{S}_{n+1} \geq q] = \mathbb{E}_{\mathcal{D}_+, \{E_i\}_{i=1}^n} \left[ \Pr_{E_{n+1}}[\tilde{S}_{n+1} \mid \mathcal{D}_+, \{E_i\}_{i=1}^n] \right] \\ &\quad (\text{from certificate}) \geq \mathbb{E}_{\mathcal{D}_+, \{E_i\}_{i=1}^n} [c^\downarrow[\beta_{n+1}, \mathcal{B}]] \end{aligned}$$

$$(\mathbb{E}[c^\downarrow[\beta, \cdot]] \geq c^\downarrow[\mathbb{E}[\beta], \cdot]) \text{ from convexity (Lemma 1)} \geq c^\downarrow[\mathbb{E}_{\mathcal{D}_+, \{E_i\}_{i=1}^n}[\beta_{n+1}], \mathcal{B}] \geq c^\downarrow[1 - \alpha, \mathcal{B}]$$

where the last inequity holds due to vanilla CP and monotonicity.  $\square$

See § D.3 for algorithm. For the clean points the guarantee holds both marginal and conditional to  $\mathcal{E}_+ = \{E_i\}_{i=1}^n \cup E_{n+1}$ . For the perturbed points, it only holds marginally over  $\mathcal{E}_+$ . In other words, the coverage probability exceeds  $c^\downarrow[\beta_{n+1}, \mathcal{B}]$  for specific  $\tilde{X}_{n+1}$ , and exceeds  $c^\downarrow[1 - \alpha, \mathcal{B}]$  on average, when  $\mathcal{E}_+$  is drawn at random. If  $\mathcal{E}_+$  is fixed the adversary can break coverage. Previous methods guarantee that if  $X_i$  is covered  $\tilde{X}_i$  also stays covered, while we guarantee that  $\tilde{X}_i$ 's are covered on average.

**Instance-wise worst case coverage.** Our Prop. 1 relies on lower bounding the worst-case  $\Pr_{\epsilon_{n+1}}[s(\tilde{\mathbf{x}}_{n+1} + \epsilon_{n+1}, y_{n+1}) \geq q]$ , for  $\tilde{\mathbf{x}}_{n+1} = \mathbf{x}_{n+1} + \delta \in \mathcal{B}(\mathbf{x}_{n+1})$  given that  $\beta_{n+1} := \Pr_{\epsilon_{n+1}}[s(\mathbf{x}_{n+1} + \epsilon_{n+1}, y_{n+1}) \geq q]$ , where  $(\mathbf{x}_{n+1}, y_{n+1})$  and  $\epsilon_{n+1}$  are realizations of  $(X_{n+1}, Y_{n+1})$  and  $E_{n+1}$ . This is conditional to  $q$  and therefore to  $\mathcal{D}_{\text{cal}} \cup \{x_{n+1}\}$  and  $\{E_i\}_{i=1}^n$ . Formally, we define a binary classifier,  $f(\mathbf{z}) = \mathbb{I}[s(\mathbf{z}, y_{n+1}) \geq q]$  and  $g(\mathbf{z}) = \mathbb{E}_{\epsilon_{n+1}}[f(\mathbf{z} + \epsilon_{n+1})]$  for which we have  $\beta_{n+1} := g(\mathbf{x}_{n+1})$ . Note that  $\mathcal{X}$  is a convex subset of  $\mathbb{R}^d$  and the score  $s(\cdot, y)$  is continuous everywhere therefore our classifier is measurable [17]. For any fixed  $\mathcal{D}_+$ , we can lower bound  $g(\tilde{\mathbf{x}}_{n+1})$  and thus  $\tilde{\beta}_{n+1} = \min_{\tilde{\mathbf{x}}_{n+1} \in \mathcal{B}(\mathbf{x}_{n+1})} g(\tilde{\mathbf{x}}_{n+1})$  with existing classification certificates, e.g. Cohen et al. [6].

**Certified lower bound  $\tilde{\beta}$ .** A smoothing binary certificate computes the bound  $c^\downarrow[g(\cdot), \mathbf{x}_{n+1}, \mathcal{B}]$  regardless of the original definition of  $f$  - mechanics of the score function or model - and only as a function of the value  $\beta = g(\mathbf{x}_{n+1})$ . We use the  $c^\downarrow[\beta, \mathcal{B}]$  notation, following Zargarbashi and Bojchevski [23]. For the known  $\mathbf{x}_{n+1}$ , a (pointwise) certified lower bound on  $g(\tilde{\mathbf{x}}_{n+1}) : \tilde{\mathbf{x}}_{n+1} \in \mathcal{B}(\mathbf{x}_{n+1})$  is obtained by searching for the worst measurable binary function  $h$  in  $\mathcal{H}$  (set of all measurable functions) such that  $h$  has the same smooth output as  $f$  at  $\mathbf{x}_{n+1}$ . Formally:

$$c^\downarrow[\beta, \mathcal{B}_r] = \min_{h \in \mathcal{H}} \Pr_{\epsilon} [h(\tilde{\mathbf{u}} + \epsilon) = 1] \quad \text{s.t.} \quad \Pr_{\epsilon} [h(\mathbf{u} + \epsilon) = 1] = \mathbb{E}_{\epsilon} [g(\mathbf{x}_{n+1})] = \beta \quad (4)$$

The pair  $(\mathbf{u}, \tilde{\mathbf{u}})$  are called canonical points. Cohen et al. [6], Yang et al. [22] discuss this in details; but intuitively, the optimization in Eq. 4 is translation (and in some cases rotation) invariant, and with the symmetries in the ball and the smoothing scheme, for any  $\mathbf{x}$ , and  $\tilde{\mathbf{x}}$  we can use a fixed set of canonical points. For  $\ell_p$  balls, and symmetric additive smoothing (including isotropic Gaussian noise) these points are one at the center, and the other at the edge (or vertex) of the ball; i.e.  $\mathbf{u} = [0, 0, \dots, 0]$ , and  $\tilde{\mathbf{u}} = [r, 0, \dots, 0]$ . For a detailed discussion also see section D.1 from Zargarbashi and Bojchevski [23]. Since the function  $f$  itself is a feasible solution to Eq. 4, it is a valid lower bound for  $g(\mathbf{x}_{n+1})$ .

<sup>2</sup>Moreover, for a fixed calibration set  $\mathcal{D}_{\text{cal}} = \{Z_i\}_{i=1}^n$ , and every draw of  $E_i$ 's under additional mild assumptions:  $\Pr[S_{n+1} \geq q \mid \mathcal{D}_{\text{cal}}, \mathcal{E}_+] \sim \text{Beta}((1 - \alpha) \cdot (n + 1), \alpha(n + 1))$ .

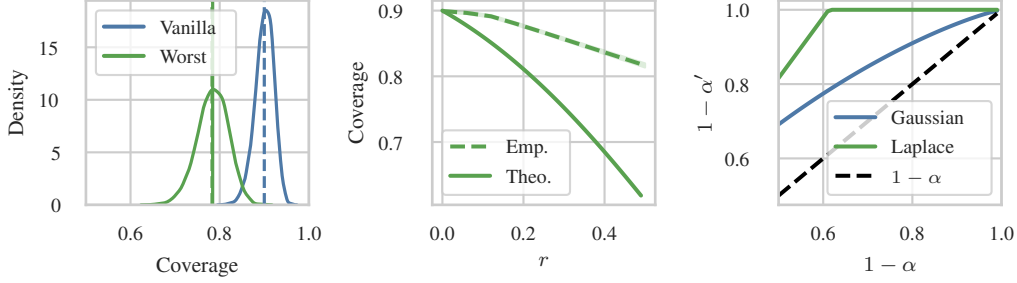


Figure 2: [Left] Samples from the beta distribution of coverage  $\beta$  and per-sample worst coverage  $\tilde{\beta}$  the dashed line is the average, and overlapping solid line is  $c^\downarrow[1 - \alpha, \mathcal{B}]$ . [Middle] The empirical, and theoretical worst case coverage. [Right] The robust  $1 - \alpha'$  for two different smoothings.

The mean-constrained binary certificate in Eq. 4 is a common problem in the randomized smoothing literature. The problem is efficiently solvable and in many cases has a closed form solution. For the isotropic Gaussian smoothing with  $\ell_2$  (and  $\ell_1$ ) ball the lower bound is  $\tilde{\beta} = \Phi_\sigma(\Phi_\sigma^{-1}(\beta) - r)$  where  $\Phi_\sigma$  is the CDF of the Gaussian distribution  $\mathcal{N}(0, \sigma)$  [15]. Using the recipe from Yang et al. [22], in § 3.1, we discuss how to compute  $c^\downarrow[p, \mathcal{B}]$  for other smoothing schemes.

**Lemma 1.**  $c^\downarrow[\beta, \mathcal{B}]$  as the solution to Eq. 4 is convex and monotonically increasing w.r.t.  $\beta$ .

We defer the proofs to § D.1. There we rigorously prove Lemma 1 directly from the definition of Eq. 4 via duality. Here we provide a sketch of an alternative proof that is insightful. Lee et al. [16] show that to solve Eq. 4, the space  $\mathcal{X}$  can be divided to (finite or infinite) regions of constant likelihood ratio  $\mathcal{R}_t = \{z : \frac{\Pr[z=\tilde{u}+\epsilon]}{\Pr[z=u+\epsilon]} = c_t\}$ . If we can sort these regions in descending order w.r.t  $c_t$ , the problem reduces to the following linear program which is a fractional knapsack problem:

$$c^\downarrow[\beta, \mathcal{B}] = \min_{\mathbf{h} \in [0,1]^T} \mathbf{h}^\top \cdot \mathbf{q} \quad \text{s.t.} \quad \mathbf{h}^\top \cdot \mathbf{p} = \beta$$

where  $T$  is number of regions,  $h_t$  is the average value of  $h(z)$  inside the region  $\mathcal{R}_t$ ,  $p_t = \Pr[u + \epsilon \in \mathcal{R}_t]$ ,  $q_t = \Pr[\tilde{u} + \epsilon \in \mathcal{R}_t]$ , and the vectors  $\mathbf{h}, \mathbf{p}, \mathbf{q}$  gather all  $h_t, p_t, q_t$ 's (see Lee et al. [16] for the derivation). W.l.o.g assume that the  $\mathbf{p}$ , and  $\mathbf{q}$  are sorted decreasingly w.r.t.  $c_t$ . The optimal solution is  $\mathbf{h}^* = [1, 1, \dots, m, 0, \dots, 0]$ , for some  $m \in (0, 1)$  which is to fill regions in order up to when  $\mathbf{h} \cdot \mathbf{p}$  reaches  $\beta$ . Each index of  $\mathbf{h}^*$  is one region being filled and by setting  $h_t^* = 1$  the  $\mathbf{h} \cdot \mathbf{q}$ , and  $\mathbf{h} \cdot \mathbf{p}$  increase by  $q_t$ , and  $p_t$ . Therefore  $c^\downarrow[\beta, \mathcal{B}] = \mathbf{h}^* \cdot \mathbf{q}$  is a continuous piecewise linear function with slope of  $q_t/p_t$  which is increasing across regions. A piecewise linear function with an increasing slope in each piece is convex. This convexity directly helps us to bound  $\mathbb{E}[c^\downarrow[\beta, \mathcal{B}]] \geq c^\downarrow[\mathbb{E}[\beta], \mathcal{B}]$ .

Note that in Prop. 1 the guarantee is over the coverage probability and independent of the setup; therefore, without any change, one can use it to make conformal regression robust. Regardless of the downstream task the certificate is always for binary classification. Furthermore, the result is not restricted to a specific scheme and can be used for any smoothing and perturbation ball (see § 3.1).

**Coverage distribution.** The coverage probability (given exchangeable scores) comes from a beta-distribution and for each sample  $\beta$  from it, the robust coverage  $\tilde{\beta}$  (under worst-case noise) is lower bounded by  $c^\downarrow[\beta, \mathcal{B}]$ . Therefore, the distribution of the robust coverage is computed by convolution of the beta-CDF and the function  $c^\downarrow[\cdot, \mathcal{B}]$  (see Fig. 2-left). The convexity helps to bound the mean of this new distribution. Our robust guarantee is however very conservative as it relies on no-information about the distribution of scores, or the inputs. Fig. 2-middle compares the worst case guarantee and the empirical performance of RCP1 (with  $\mathcal{C}_0$ ) under adversarial attack.

**Obtaining nominal coverage.** Prop. 1 says that under perturbation, the coverage guarantee over smooth inference decreases at most by  $c^\downarrow[1 - \alpha, \mathcal{B}]$ . A simple solution to attain  $1 - \alpha$  robust coverage is to set the nominal coverage to a value  $1 - \alpha'$  such that  $c^\downarrow[1 - \alpha', \mathcal{B}] \geq 1 - \alpha$ . From Zargarbashi and Bojchevski [23] (Lemma 3) we know that in many of the smoothing schemes, we have  $c^\uparrow[c^\downarrow[p, \mathcal{B}], \mathcal{B}^{-1}] = p$ . Therefore, to attain  $1 - \alpha$  robust coverage, we only need to set the threshold as the  $c^\uparrow[1 - \alpha, \mathcal{B}^{-1}]$  quantile of the calibration scores (see Fig. 2-right).

### 3.1 Robust Conformal Sets with Randomized Smoothing of All Shapes and Sizes

Both RCP1, and BinCP work with any smoothing and ball  $\mathcal{B}$ . However, some binary certificates are given as a robust radius  $r^*$  – the radius up to which the prediction remains the same,  $c^\perp[p, \mathcal{B}_{r^*}] = 0.5$ . Yang et al. [22] provide a recipe to compute the  $r^*$  for general  $\ell_p$  certificate under additive randomized smoothing. Further they compute closed form radii for Gaussian, Laplace, and uniform smoothing as examples. We tweak their “differential” method to derive probability bounds:

**Proposition 2.** *For a binary classifier  $f(\mathbf{x})$ , and an additive smoothing function  $\xi$ , let  $g(\mathbf{x}) := \Pr_{\epsilon \sim \xi}[f(\mathbf{x} + \epsilon) = 1]$ . Let  $\mathcal{U} = \{\mathbf{x} : f(\mathbf{x}) = 1\}$  be the decision boundary and  $\mathcal{U} - \mathbf{z}$  as the same set translated from  $\mathbf{z}$  to the origin. For the smoothing distribution  $\xi$ , let  $\xi(\mathcal{U}) = \Pr_{\epsilon \sim \xi}[\epsilon \in \mathcal{U}]$  be the expectation of the decision boundary under smoothing, define:*

$$\Omega(\beta) := \sup_{\delta: \|\delta\|=1} \sup_{\mathcal{U} \in \mathbb{R}^d: \xi(\mathcal{U})=\beta} \lim_{r \rightarrow 0^+} \frac{\xi(\mathcal{U} - r\delta) - \beta}{r}$$

where  $\beta = \xi(\mathcal{U} - \mathbf{x}) = \mathbb{E}[f(\mathbf{x} + \epsilon)]$ . Defining the function  $F(\beta) = \int_\beta^{1/2} \frac{1}{\Omega(p)} dp$ , for all  $r \leq F(\beta)$ :

$$c^\uparrow[\beta, \mathcal{B}_r] = \sup \{\beta' : F(\beta') \geq F(\beta) - r\} \quad (5)$$

Similarly, for all  $r \leq F(1 - \beta)$  we have  $c^\perp[\beta, \mathcal{B}_r] = \inf \{\beta' : F(1 - \beta') \leq F(1 - \beta) + r\}$ .

The function  $1/\Omega(p)$  encodes the minimum perturbation to make an infinitesimal increase in the expectation of the worst-case classifier [22]. Intuitively, the differential approach uses the line integral to bound the changes in the function  $g(\mathbf{x})$  when moving to  $g(\tilde{\mathbf{x}})$ . One way to obtain the bound is compute the closed form of  $\Omega(p)$  for the smoothing and find  $\bar{\beta}$  in  $\int_\beta^{\bar{\beta}} \frac{1}{\Omega(p)} dp \leq r$ . Yang et al. [22] derive the closed form of  $\Omega(p)$  (originally written as  $\Phi(p)$ ) for various distributions. We can also directly use their result  $F(\beta)$ , and find the upper bound via binary search.

### 3.2 Extension to Conformal Risk Control

Similar to our robust CP, we can use robustness certificates to define smoothing-based robust risk control. For a risk function  $\mathcal{L}(\mathbf{x}_i, \lambda)$  over exchangeable  $\{\mathbf{x}_i\}_{i=1}^{n+1}$  that is non-decreasing to  $\lambda$ , bounded  $\mathcal{L}(\mathbf{x}, \lambda) \in [a, b]$  and right continuous, Angelopoulos et al. [1] guarantee the following:

$$\mathbb{E}_{\{\mathbf{x}_i\}_{i=1}^{n+1}}[\mathcal{L}(\mathbf{x}_{n+1}, \lambda^*)] \leq \alpha \quad \text{for} \quad \lambda^* = \inf \left\{ \lambda : \frac{\sum_{i=1}^n \mathcal{L}(\mathbf{x}_i, \lambda) + b}{n+1} \leq \alpha \right\}$$

Here  $\alpha \in [a, b]$  is any user adjusted risk level. Similar to conformal prediction, we can also define a randomly augmented risk function  $\mathcal{L}(\mathbf{x}_i + \epsilon, \lambda)$ . The noise does not break the exchangeability and therefore  $\mathbb{E}_{\{\mathbf{x}_i\}_{i=1}^{n+1}, \epsilon}[\mathcal{L}(\mathbf{x}_{n+1} + \epsilon, \lambda^*)] \leq \alpha$  for the  $\lambda^*$  computed on the randomly augmented calibration set. Here due to the continuous nature of the risk function we use confidence certificates:

$$c_c^\uparrow[\beta, \mathcal{B}] = \max_{h \in \mathcal{H}} \mathbb{E}[h(\tilde{\mathbf{x}}_{n+1})] \quad \text{s.t.} \quad \mathbb{E}[h(\mathbf{x}_{n+1})] \leq \beta$$

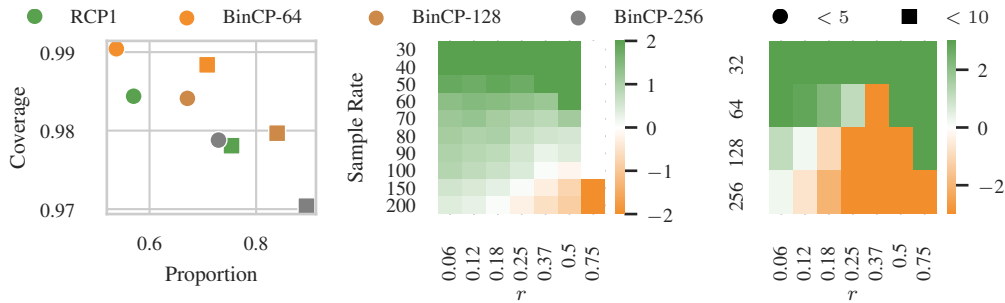


Figure 3: [Left] Proportion, and coverage of the prediction sets with  $\leq 5$ , and  $\leq 10$  elements for the ViT model. [Middle]  $|C_{r, \text{BinCP}}| - |C_{r, \text{RCP1}}|$  for the CIFAR-10 dataset with a ResNet model. [Right] ImageNet dataset and ViT models ( $r = 0.25$ ). In all plots  $\sigma = 0.5$  and RCP1 uses a single sample.

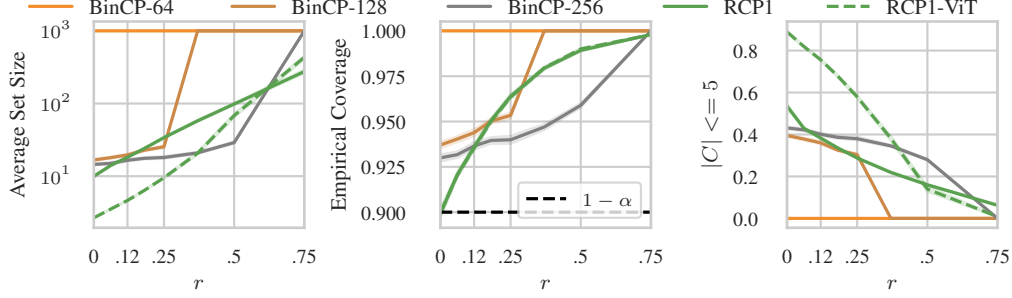


Figure 4: On ImageNet, cheap setup with  $\sigma = 0.5$ : [Left] Compares the average set size of BinCP with various sample rates to RCP1. [Middle] the empirical coverage. [Right] proportion of prediction sets with size less than 5 elements. Dashed line is the result of the ViT model with the same  $\sigma$ .

Similarly, this problem can be efficiently solved, and for the Gaussian distribution it has a closed form solution of  $b \cdot \Phi_\sigma(\Phi_\sigma^{-1}(\frac{\beta-a}{b-a}) + r) - a(1 - \Phi_\sigma(\Phi_\sigma^{-1}(\frac{\beta-a}{b-a}) + r))$ . With  $[a, b] = [0, 1]$  (e.g. in false negative rate) the closed form is identical to the classification certificate [15].

## 4 Experiments

Our metrics are average set size (lower is better), and empirical coverage (close to but exceeding  $1 - \alpha$  on average). As BinCP [23] outperforms other robust CP approaches [24, 21], we set it as the main comparison baseline. Originally, BinCP is designed to decrease the required sample rate for efficient (small) robust sets. All recent RCPs return non-informative sets for low number of samples (e.g.  $\leq 64$ ). Note that our main contribution is to return efficient sets with one inference per input; therefore we do not expect RCP1 to outperform BinCP for a large sample-rate. Our reported results are over 100 iterations with calibration set randomly sampled from the data. Further details are in § E.

**Classification.** We compare methods for the CIFAR10, and ImageNet datasets. We have two inference pipelines. As in the original pipeline from BinCP, and CAS, we use the ResNet models trained with noise augmentation from Cohen et al. [6]. We call this the computationally cheap setup, where large sample-rates, although inefficient, are not unrealistic. We use an alternative more expensive pipeline outlined by Carlini et al. [5], where the input is first denoised by a diffusion model and then classified by a vision transformer. For CIFAR-10 we combine a 50M-parameter diffusion model from Dhariwal and Nichol [8], with a ViT-B/16 from Dosovitskiy et al. [9], pretrained on ImageNet at  $224 \times 224$  resolution and finetuned on CIFAR10 with 97.9% accuracy for the HuggingFace implementation. For ImageNet we use a 552M-parameter class-unconditional diffusion model followed by BEiT-L model (305M parameters) from Bao et al. [3] achieving 88.6% top-1 validation accuracy. We use the implementation provided by the timm library [20].

**Smaller set sizes.** Increasing the sample-rate in BinCP decreases the set size. In Fig. 1-middle we compare BinCP and RCP1 on set size and computation time for the ImageNet dataset. On the same setup, RCP1 is similar in set size to BinCP with 64 to 128 inferences per point (see Fig. 3-middle, and right). Indeed bypassing the MC sampling saves us a significant time. We can also compete in set size by using a better yet compute-heavy model (e.g. a combination of diffusion for denoising and ViT). The overhead of RCP1 applied on a larger model is considerably less than BinCP with ResNet due to the many forward passes. Fig. 3-, and Fig. 6-compare methods across different radii for the CIFAR-10 and ImageNet datasets. Our complete comparison on this experiment is in § E. Note that it is significantly inefficient to run  $\geq 100$  forwards passes per image on the ViT models. Additionally, we use the results in § 3.1 to show that the method works similarly for any smoothing scheme and threat model. For that we show the performance of BinCP (under two sample rates) and RCP1 for the  $\ell_1$  ball under uniform smoothing distribution in Fig. 5-right.

For a dataset like ImageNet (with 1000 classes), the average set size alone is not a measure of usability. Consider a CP returning 50% singleton sets and  $|\mathcal{Y}|$  for the rest, compared to a CP returning sets of size 100 for all inputs. Surely, the latter option is not usable even though it has smaller average set size. Hence, we also report the proportion of the prediction sets with less than 5 elements in

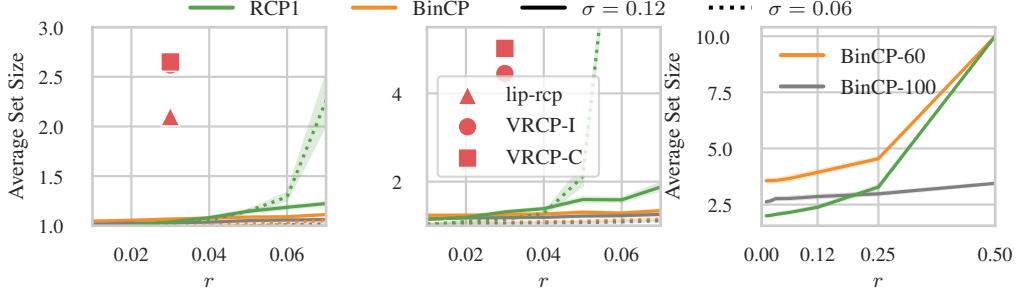


Figure 5: Performance on smaller radii in comparison with non-smoothing RCPs [14, 17] for CIFAR-10 and a ViT model. [Left]  $1 - \alpha = 0.9$ , and [Middle]  $1 - \alpha = 0.95$ . Smoothing is better. [Right] Performance of the methods for a Uniform- $\ell_1$  certificate for  $\epsilon \sim \text{Uniform}[-1/\sqrt{3}, 1/\sqrt{3}]$ .

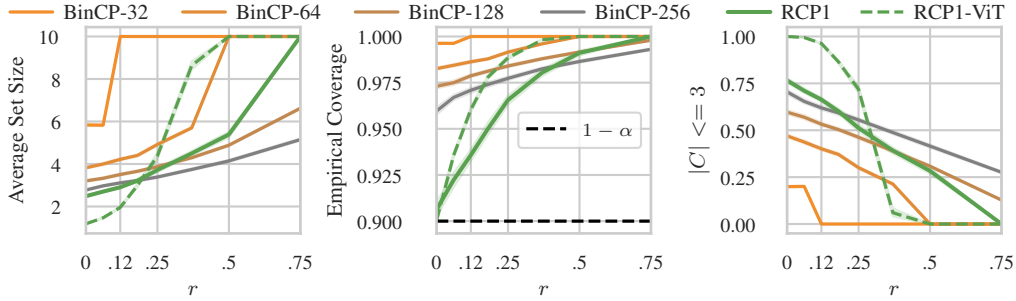


Figure 6: On CIFAR-10, ResNet model with  $\sigma = 0.5$ : [Left] The average set size compared to BinCP (with various sample rates), RCP1 [Middle] the empirical coverage, and [Right] proportion of sets with less than 3 labels. Dashed line shows the ViT model (with  $\sigma = 0.25$ ).

Fig. 4-right (also see § E). This metric is only trustworthy if we do not sacrifice coverage for smaller sets. In Fig. 3-left we show that these sets have coverage larger than  $1 - \alpha$ .

**Small radii.** Jeary et al. [14], and Massena et al. [17] propose RCP using verifiers and Lipschitz constant of the network. Although their result is for one order of magnitude smaller radii (e.g. 0.02 instead of 0.25), their methods are efficient by using one forward per input. With RCP1 being the same in that metric, we compare with them in Fig. 5-left and middle reporting performance on smaller radii. Aside better performance, RCP1 has a black-box access and works for any model. Intuitively, as shown in Fig. 1-left, smooth (or augmented) inference is significantly more robust to perturbations.

**Time-comparison.** With  $t_{\text{cert}}$  and  $t_f$  as the time of computing bounds, and model’s inference time, other smoothing based RCPs at best require  $\mathcal{O}(n_{\text{mc}} \times \mathcal{D}_{\text{cal}} \times t_f + t_{\text{cert}})$  for calibration where  $n_{\text{mc}}$  is the number of MC samples. For each test point they also require  $\mathcal{O}(n_{\text{mc}} \times t_f)$  time. RCP1 takes the same time as the normal model’s inference plus an additional  $\mathcal{O}(t_{\text{cert}})$  for calibration. Similarly, RCP1 takes  $n_{\text{mc}}$  less memory compared to other smoothing RCPs. We show the runtime of the ViT pipeline for the used datasets in Table 1. Note that this is only the time to compute logits as the other processes (including certificates) are negligible compared to it. The runtime of BinCP with a sample rate comparable to RCP1 is significantly high for large models like ViT; for instance, RCP1 and a comparable BinCP (with 128 samples on ImageNet) need  $\sim 2'46''$ , and  $\sim 5\text{h } 55'$  to process 5000 images.

Table 1: Estimated runtimes (in HH:MM:SS) for 1000 inputs using an H-100 GPU. Results are scaled from a full experimental run assuming a linear cost in both the number of inputs and samples.

Pipeline	Dataset	1 Sample	64 Samples	128 Samples	256 Samples
ViT	CIFAR-10	0:00:01	0:01:09	0:02:19	0:04:39
	ImageNet	0:00:33	0:35:30	1:11:00	2:22:01

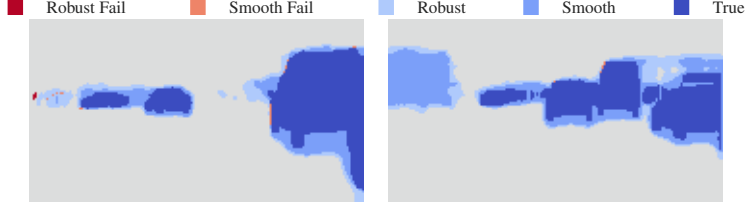


Figure 7: Performance of vanilla and robust risk control. From lighter to darker the colors are robust region, vanilla (non-robust) region, and the ground truth region. Here  $\sigma = 0.25$ , and  $r = 0.06$ .

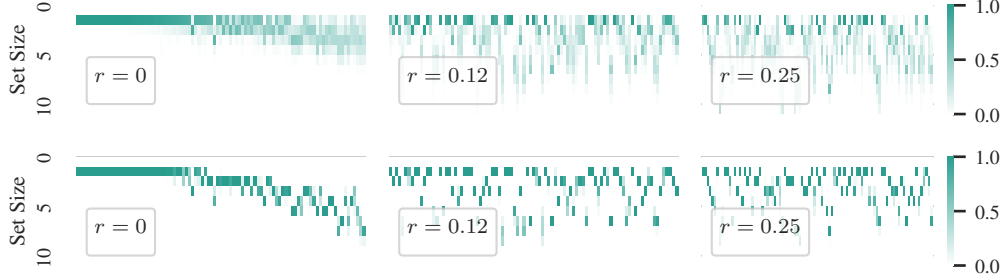


Figure 8: Randomness in set sizes for a CIFAR-10 dataset and ResNet model. The  $x$ -axis sorts datapoints in a fixed order (same across all plots), and the  $y$  axis shows the set size. The intensity of pixels shows the probability of a specific set size for that point over  $\epsilon$ . [Top] shows RCPI, and [Bottom] BinCP (150 samples). RCPI has larger variance compared to BinCP.

**Robust conformal risk control.** We use the model from Fischer et al. [10] on the CityScapes dataset [7] which is a scene segmentation task. We mask the regions where a target class (e.g. car) might be present. The error function is the false negative ratio (FNR) – the portion of the pixels from the target class that is not masked. We take the  $\exp(f(x))_y$  as the score of the class  $y$ , and we set the mask as  $\mathbb{I}[\exp(f(x))_y \geq 1 - \lambda]$ . Note that here the classes could possibly overlap. We calibrate by finding a  $\lambda$  that results in a FNR loss less than the user adjusted tolerable risk. So far this is the first result for smoothing-based robust conformal risk control. The process of robust risk control is similar to robust CP. We first smooth the image data (only for one sample), then we compute the  $\lambda$  that results in  $c_c^*[\alpha, \mathcal{B}]$  risk. We report the results in Table 2, and show an example in Fig. 7.

**Limitation: Increased variance.** As in Fig. 8, RCPI shows considerably more randomness in the prediction sets compared to BinCP. This is essentially due to the random definition of the prediction set and the score function – the prediction set in RCPI is a function of the random variable  $\epsilon$ . This randomness does not affect the final robust / vanilla coverage.

## 5 Conclusion

Smoothing-based robust CP methods can return small prediction sets robust to large radii, however, their limitation is that they need many forward passes per input. Instead, we show that noise-augmented inference combined with CP is inherently robust, and we propose RCPI which needs only one forward pass per input. Our approach returns sets with size similar to state of the art while nullifying the need of many MC samples. We further extend our method to conformal risk control.

Table 2: Risk and mask size for the Cityscapes dataset. Risk level is 0.15, with 100 calibration points. The variance is not over calibration sampling but over the images and  $r = 0.06$ .

Class	Risk	Robust Risk	(True) Class Prop.	Mask Prop.	Robust Mask Prop.
Pedestrian	$0.1474 \pm 0.2797$	$0.1111 \pm 0.2588$	$0.0160 \pm 0.0279$	$0.1891 \pm 0.1257$	$0.2522 \pm 0.1312$
Car	$0.1466 \pm 0.2582$	$0.0833 \pm 0.2032$	$0.0539 \pm 0.0545$	$0.0832 \pm 0.0733$	$0.1101 \pm 0.0807$

## References

- [1] Anastasios N Angelopoulos, Stephen Bates, Adam Fisch, Lihua Lei, and Tal Schuster. Conformal risk control. *arXiv preprint arXiv:2208.02814*, 2022.
- [2] Anastasios N Angelopoulos, Rina Foygel Barber, and Stephen Bates. Theoretical foundations of conformal prediction. *arXiv preprint arXiv:2411.11824*, 2024.
- [3] Hangbo Bao, Li Dong, Songhao Piao, and Furu Wei. Beit: Bert pre-training of image transformers. *arXiv preprint arXiv:2106.08254*, 2021.
- [4] Aleksandar Bojchevski, Johannes Gasteiger, and Stephan Günnemann. Efficient robustness certificates for discrete data: Sparsity-aware randomized smoothing for graphs, images and more. In *International Conference on Machine Learning*, pages 1003–1013. PMLR, 2020.
- [5] Nicholas Carlini, Florian Tramer, Krishnamurthy Dj Dvijotham, Leslie Rice, Mingjie Sun, and J Zico Kolter. (certified!!) adversarial robustness for free! *arXiv preprint arXiv:2206.10550*, 2022.
- [6] Jeremy Cohen, Elan Rosenfeld, and Zico Kolter. Certified adversarial robustness via randomized smoothing. In *international conference on machine learning*, pages 1310–1320. PMLR, 2019.
- [7] Marius Cordts, Mohamed Omran, Sebastian Ramos, Timo Rehfeld, Markus Enzweiler, Rodrigo Benenson, Uwe Franke, Stefan Roth, and Bernt Schiele. The cityscapes dataset for semantic urban scene understanding. In *Proc. of the IEEE Conference on Computer Vision and Pattern Recognition (CVPR)*, 2016.
- [8] Prafulla Dhariwal and Alexander Nichol. Diffusion models beat gans on image synthesis. *Advances in neural information processing systems*, 34:8780–8794, 2021.
- [9] Alexey Dosovitskiy, Lucas Beyer, Alexander Kolesnikov, Dirk Weissenborn, Xiaohua Zhai, Thomas Unterthiner, Mostafa Dehghani, Matthias Minderer, Georg Heigold, Sylvain Gelly, et al. An image is worth 16x16 words: Transformers for image recognition at scale. *arXiv preprint arXiv:2010.11929*, 2020.
- [10] Marc Fischer, Maximilian Baader, and Martin Vechev. Scalable certified segmentation via randomized smoothing. In *International Conference on Machine Learning*, pages 3340–3351. PMLR, 2021.
- [11] Asaf Gendler, Tsui-Wei Weng, Luca Daniel, and Yaniv Romano. Adversarially robust conformal prediction. In *International Conference on Learning Representations*, 2021.
- [12] Subhankar Ghosh, Yuanjie Shi, Taha Belkhouja, Yan Yan, Janardhan Rao Doppa, and Brian Jones. Probabilistically robust conformal prediction. In *Conference on Uncertainty in Artificial Intelligence*, 2023. URL <https://api.semanticscholar.org/CorpusID:260334753>.
- [13] Chuan Guo, Geoff Pleiss, Yu Sun, and Kilian Q. Weinberger. On calibration of modern neural networks. In *International Conference on Machine Learning*, 2017. URL <https://api.semanticscholar.org/CorpusID:28671436>.
- [14] Linus Jeary, Tom Kuipers, Mehran Hosseini, and Nicola Paoletti. Verifiably robust conformal prediction. 2024.
- [15] Aounon Kumar, Alexander Levine, Soheil Feizi, and Tom Goldstein. Certifying confidence via randomized smoothing. *Advances in Neural Information Processing Systems*, 33:5165–5177, 2020.
- [16] Guang-He Lee, Yang Yuan, Shiyu Chang, and Tommi Jaakkola. Tight certificates of adversarial robustness for randomly smoothed classifiers. *Advances in Neural Information Processing Systems*, 32, 2019.
- [17] Thomas Massena, Léo Andéol, Thibaut Boissin, Corentin Friedrich, Franck Mamalet, Mathieu Serrurier, and Sébastien Gerchinovitz. Efficient robust conformal prediction via lipschitz-bounded networks. 2025.

- [18] Hadi Salman, Jerry Li, Ilya Razenshteyn, Pengchuan Zhang, Huan Zhang, Sebastien Bubeck, and Greg Yang. Provably robust deep learning via adversarially trained smoothed classifiers. *Advances in neural information processing systems*, 32, 2019.
- [19] Vladimir Vovk, Alexander Gammerman, and Glenn Shafer. Algorithmic learning in a random world. 2005.
- [20] Ross Wightman. Pytorch image models. <https://github.com/rwightman/pytorch-image-models>, 2019.
- [21] Ge Yan, Yaniv Romano, and Tsui-Wei Weng. Provably robust conformal prediction with improved efficiency. *arXiv preprint arXiv:2404.19651*, 2024.
- [22] Greg Yang, Tony Duan, J Edward Hu, Hadi Salman, Ilya Razenshteyn, and Jerry Li. Randomized smoothing of all shapes and sizes. In *International Conference on Machine Learning*, pages 10693–10705. PMLR, 2020.
- [23] Soroush H Zargarbashi and Aleksandar Bojchevski. Robust conformal prediction with a single binary certificate. 2025.
- [24] Soroush H Zargarbashi, Mohammad Sadegh Akhondzadeh, and Aleksandar Bojchevski. Robust yet efficient conformal prediction sets. In *Forty-first International Conference on Machine Learning*, 2024.
- [25] Dinghuai Zhang, Mao Ye, Chengyue Gong, Zhanxing Zhu, and Qiang Liu. Black-box certification with randomized smoothing: A functional optimization based framework. *Advances in Neural Information Processing Systems*, 33:2316–2326, 2020.

## A Related Work

Gendler et al. [11] initially proposed robust CP resilient to adversarial examples (worst-case noise) without accounting for finite samples (asymptotically valid setup). Yan et al. [21] added finite sample correction and proposed a new score to return (set size) efficiency. Both mentioned works were using randomized smoothing and the mean of the smooth score to bound the worst case perturbations. Zargarbashi et al. [24] (CAS) proposed to use the CDF information of the smooth score – a more restrictive constraint and therefore returned smaller prediction sets. All of these methods required unrealistically expensive setup with  $10^4$  MC samples to be able to return acceptably small sets. Zargarbashi and Bojchevski [23] (BinCP) defined a quantile-based score over the distribution of the smooth scores, that allowed same set size as CAS with orders of magnitude less samples (e.g. 200 would be sufficient). In contrast with all of the methods RCP1 works with a single augmented sample and without involving finite sample correction, which lies at the computation efficiency side of this trade-off.

Orthogonal to randomized smoothing, Jeary et al. [14], and Massena et al. [17] use verifiers and Lipschitz continuity of the networks to bound the score function. Their robust radii is one order of magnitude smaller than smoothing RCP, but instead they do not require many forward passes per input. In Fig. 5 we show that our approach (with the same computational efficiency) provides smaller prediction sets outperforming their results; plus, our approaches works for any black-box model. Notably all mentioned works provide robustness to the worst-case noise which is orthogonal to probabilistically robust CP Ghosh et al. [12].

## B Additional Description of Figures

**Plot. 1-left.** We report how the empirical coverage of  $\mathcal{C}_0$  (dashed lines) breaks for smooth prediction in BinCP and randomized augmented score in RCP1, compared to the vanilla conformal prediction (red dashed line). In all cases, we calibrate over clean calibration set and for radii  $r$  we return the prediction set of  $\tilde{x}_{n+1}$  which is  $x_{n+1}$  perturbed with adversarial attacks. Specifically we use the PGDSmooth attack from [18] for smooth methods and conventional PGD attack for vanilla CP. Compared to PGD, the PGDSmooth attack performs stronger for smooth scores. The solid lines show the empirical coverage of  $\mathcal{C}_r$  from BinCP and RCP1 on the same adversarial data. The main takeaway of the figure is to show the robustness of  $\mathcal{C}_r$ , and the inherent resilience of smooth and augmented inference to the adversarial (worst-case) noise. The result is for CIFAR-10 dataset, ResNet model and  $\sigma = 0.5$ .

**Plot. 1-middle.** We compared the robust set size of BinCP and RCP1; we plotted  $|\mathcal{C}_{r,\text{BinCP}}| - |\mathcal{C}_{r,\text{RCP1}}|$  for which lower is better. The plot is for CIFAR-10 dataset, ResNet model and  $\sigma = 0.5$ .

**Plot. 1-right.** Each point is a computation of  $\mathcal{C}_r$  shown both in time and set size. All times are divided by a single inference of the ResNet model. Here we evaluated two forward pipelines of cheaper ResNet model, and more time costly diffusion + vision transformer (as discussed in § 4). Both axis are log-scale and the plot is for the ImageNet dataset. Here  $\sigma = 0.5$ .

**Plot. 2-left.** We took samples from the Beta distribution of the coverage – each sample is then a number  $\beta$ . We computed the  $c^\downarrow[\beta, \mathcal{B}]$  and draw a distribution of the new values. For the Beta distribution, we have  $n = 200$ , and  $1 - \alpha = 0.9$ . For the  $c^\downarrow$  function we used  $\sigma = 0.5$ , and  $r = 0.25$ .

**Plot. 2-middle.** We show the empirical coverage value under the PGDSmooth attack with  $\sigma = 0.5$  over various radii. We use the same sigma to show the theoretical lower bound coverage.

**Plot. 2-right.** We reported the  $c^\downarrow$  function for Gaussian and Laplace smoothing both with  $\sigma = 0.5$ . The plots are not empirical.

**Plot. 5-right.** Here we use the  $\ell_1$  certificate from Yang et al. [22]. Here the smoothing scheme is  $\epsilon = \text{Uniform}[-\sigma/\sqrt{3}, \sigma/\sqrt{3}]$ .

## C More on Conformal Prediction

Our default score function in the manuscript is TPS (threshold prediction sets) where the score function is directly set to the softmax;  $s(x, y) = \text{Softmax}_y(f(x))$  for the prediction model  $f$ . Another choice

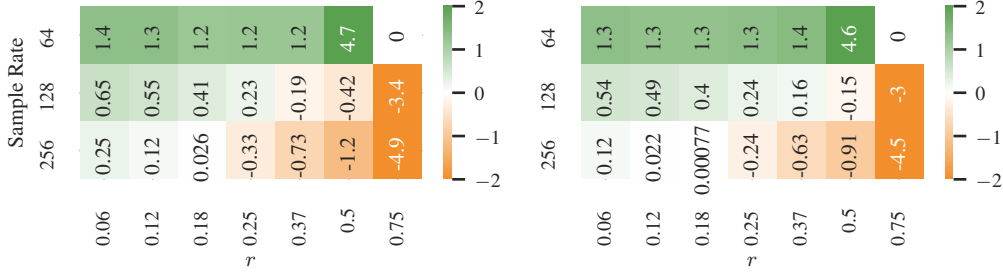


Figure 9: Comparison of BinCP and RCP1 for [Left] TPS, and [Right] APS score function on CIFAR-10 dataset with  $\sigma = 0.9$ .

Table 3: Set size of RCP1 for TPS and APS score across radii ( $r$ ) and target coverage guarantees.

$r$	Coverage	TPS		APS	
		Avg Set Size	Emp. Cov.	Avg Set Size	Emp. Cov.
0.06	0.85	$2.17 \pm 0.02$	$0.88 \pm 0.00$	$2.52 \pm 0.03$	$0.88 \pm 0.00$
	0.90	$2.70 \pm 0.03$	$0.92 \pm 0.00$	$2.98 \pm 0.02$	$0.92 \pm 0.00$
	0.95	$3.74 \pm 0.01$	$0.97 \pm 0.00$	$3.91 \pm 0.04$	$0.97 \pm 0.00$
0.12	0.85	$2.44 \pm 0.03$	$0.90 \pm 0.00$	$2.76 \pm 0.02$	$0.90 \pm 0.00$
	0.90	$2.93 \pm 0.04$	$0.94 \pm 0.00$	$3.23 \pm 0.01$	$0.94 \pm 0.00$
	0.95	$3.96 \pm 0.06$	$0.97 \pm 0.00$	$4.07 \pm 0.04$	$0.97 \pm 0.00$
0.18	0.85	$2.70 \pm 0.04$	$0.92 \pm 0.00$	$2.99 \pm 0.01$	$0.92 \pm 0.00$
	0.90	$3.25 \pm 0.05$	$0.95 \pm 0.00$	$3.44 \pm 0.03$	$0.95 \pm 0.00$
	0.95	$4.48 \pm 0.09$	$0.98 \pm 0.00$	$4.48 \pm 0.02$	$0.98 \pm 0.00$
0.25	0.85	$3.03 \pm 0.01$	$0.94 \pm 0.00$	$3.33 \pm 0.04$	$0.94 \pm 0.00$
	0.90	$3.70 \pm 0.02$	$0.97 \pm 0.00$	$3.89 \pm 0.03$	$0.97 \pm 0.00$
	0.95	$4.81 \pm 0.01$	$0.99 \pm 0.00$	$4.82 \pm 0.04$	$0.99 \pm 0.00$
0.37	0.85	$3.62 \pm 0.06$	$0.96 \pm 0.00$	$3.91 \pm 0.01$	$0.97 \pm 0.00$
	0.90	$4.48 \pm 0.03$	$0.98 \pm 0.00$	$4.55 \pm 0.09$	$0.98 \pm 0.00$
	0.95	$6.24 \pm 0.14$	$0.99 \pm 0.00$	$6.49 \pm 0.04$	$1.00 \pm 0.00$
0.50	0.85	$4.51 \pm 0.03$	$0.98 \pm 0.00$	$4.55 \pm 0.11$	$0.98 \pm 0.00$
	0.90	$5.32 \pm 0.04$	$0.99 \pm 0.00$	$5.34 \pm 0.03$	$0.99 \pm 0.00$
	0.95	$10.00 \pm 0.00$	$1.00 \pm 0.00$	$10.00 \pm 0.00$	$1.00 \pm 0.00$
0.75	0.85	$6.28 \pm 0.19$	$0.99 \pm 0.00$	$6.31 \pm 0.11$	$0.99 \pm 0.00$
	0.90	$10.00 \pm 0.00$	$1.00 \pm 0.00$	$10.00 \pm 0.00$	$1.00 \pm 0.00$
	0.95	$10.00 \pm 0.00$	$1.00 \pm 0.00$	$10.00 \pm 0.00$	$1.00 \pm 0.00$

is to use the logits of the model as the conformity score  $s(\mathbf{x}, y) = f(\mathbf{x})_y$ . Similar to BinCP we are using a single binary certificate which do not rely on bounded score function. Another conformal prediction method called as adaptive prediction sets (APS) uses the accumulated softmax up to label  $y$  as the conformity score; formally  $s(\mathbf{x}, y) = -[\pi(\mathbf{x}, y) \cdot u + \sum_{k=1}^{|\mathcal{Y}|} \pi(\mathbf{x}, y_k) \cdot \mathbb{I}[\pi(\mathbf{x}, y_k) > \pi(\mathbf{x}, y)]]$  where  $\pi(\mathbf{x}, y) = \text{Softmax}_y(f(\mathbf{x}))$  and  $u \sim \text{Uniform}[0, 1]$ . While this score results in larger sets, it increases adaptivity – approximate conditional coverage.

We report the result using these score functions in Fig. 9 (comparison of BinCP and RCP1 for each score) and Table 3 (the set size of RCP1 for both score functions). As expected, similar trend as TPS is observed for APS as well.

Same as BinCP we also do not need the score function to be bounded. However in the end, using an unbounded score function (like using logits directly) did not show to improve over the existing APS and TPS.

## D Supplementary to Theory

### D.1 Proofs

*Proof of Lemma 1.* The Lagrangian form of Eq. 4 is:

$$\begin{aligned}\mathcal{L}(\beta, \lambda) &= \Pr_{\epsilon}[h(\tilde{\mathbf{u}} + \epsilon) = 1] - \lambda \left( \Pr_{\epsilon}[h(\mathbf{u} + \epsilon) = 1] - \beta \right) \\ &= E_{\mathbf{z} \sim q}[h(\mathbf{z})] - \lambda \cdot E_{\mathbf{z} \sim p}[h(\mathbf{z}) - \beta] = \lambda \cdot \beta + E_{\mathbf{z} \sim q}[h(\mathbf{z})] - E_{\mathbf{z} \sim p}[h(\mathbf{z})] \\ &= \lambda \cdot \beta + \min_{h \in \{0,1\}^{|\mathcal{X}|}} \int_{\mathcal{X}} (q(\mathbf{z}) - \lambda \cdot p(\mathbf{z})) \cdot h(\mathbf{z}) d\mathbf{z}\end{aligned}$$

where  $p$  and  $q$  are smoothing distributions centered at  $\mathbf{u}$  and  $\tilde{\mathbf{u}}$  respectively. The worst classifier (the minimizer of the problem) can be derived as follows

$$h(\mathbf{z}) = \begin{cases} 0 & \text{if } q(\mathbf{z}) - \lambda \cdot p(\mathbf{z}) \geq 0 \\ 1 & \text{otherwise} \end{cases}$$

Intuitively, to minimize the term  $\int_{\mathcal{X}} (q(\mathbf{z}) - \lambda \cdot p(\mathbf{z})) \cdot h(\mathbf{z}) d\mathbf{z}$  we look at each point independently. For each point if the term  $(q(\mathbf{z}) - \lambda \cdot p(\mathbf{z}))$  is positive we cancel it by  $h = 0$  and if negative we keep it to decrease the total integral value. The resulting dual with the dual variable  $\lambda \geq 0$  is then:

$$\mathcal{L}(\beta, \lambda) = \lambda \cdot \beta + \int \min\{0, p(\mathbf{z}) - \lambda \cdot q(\mathbf{z})\} d\mathbf{z} = \lambda \cdot \beta + l(\lambda)$$

Here  $l(\lambda) := \int \min\{0, p(\mathbf{z}) - \lambda \cdot q(\mathbf{z})\} d\mathbf{z}$  is only a function of  $\lambda$ . Maximizing over  $\lambda$  we get the optimal dual solution which equals the optimal primal since it was shown that strong duality holds [25]:

$$c^\downarrow[\beta, \mathcal{B}] = \max_{\lambda} \lambda \cdot \beta + l(\lambda)$$

Which is pointwise maximum of affine functions and therefore convex in  $\beta$ .

The monotonicity w.r.t.  $\beta$  directly follows from the definition. By increasing  $\beta$  the feasible space reduces to a nested subset of the previous problem which means that the solution will be greater than or equal to the original solution.  $\square$

### D.2 Lower and Upper Bounds for All Shapes and Sizes

**Lemma 2.** For a binary classifier  $f(\mathbf{x})$ , let  $g(\mathbf{x}) = \Pr_{\epsilon}[f(\mathbf{x} + \epsilon) = 1]$  and

$$g(\tilde{\mathbf{x}}) \geq c_g^\downarrow[p, \mathcal{B}] := \min_{h \in \mathcal{H}} \Pr_{\epsilon}[h(\tilde{\mathbf{x}} + \epsilon) = 1] \quad \text{s.t. } \Pr_{\epsilon}[h(\mathbf{x} + \epsilon) = 1] = g(\mathbf{x}) = p$$

Similarly let

$$g(\tilde{\mathbf{x}}) \leq c_g^\uparrow[p, \mathcal{B}] := \max_{h \in \mathcal{H}} \Pr_{\epsilon}[h(\tilde{\mathbf{x}} + \epsilon) = 1] \quad \text{s.t. } \Pr_{\epsilon}[h(\mathbf{x} + \epsilon) = 1] = g(\mathbf{x}) = p$$

Both be obtainable at the same canonical points. We have  $c_g^\uparrow[p, \mathcal{B}] = 1 - c_g^\downarrow[1 - p, \mathcal{B}]$ .

*Proof.* For simpler notation let  $\bar{g}(\mathbf{x}) = c_g^\uparrow[g(\mathbf{x}), \mathcal{B}^{-1}]$ ,  $\underline{g}(\mathbf{x}) = c_g^\downarrow[g(\mathbf{x}), \mathcal{B}^{-1}]$ , then we have

$$\begin{aligned}1 - \bar{g}(\mathbf{x}) &= 1 - \max_{h \in \mathcal{H}} \Pr_{\epsilon}[h(\tilde{\mathbf{x}} + \epsilon) = 1] \\ &\quad \text{Let } h'(\mathbf{x}) = 1 - h(\mathbf{x}) \text{ then} \\ &= 1 - \max_{h' \in \mathcal{H}} \Pr_{\epsilon}[1 - h'(\tilde{\mathbf{x}} + \epsilon) = 1] = \min_{h' \in \mathcal{H}} \Pr_{\epsilon}[h'(\tilde{\mathbf{x}} + \epsilon) = 1]\end{aligned}$$

The constraint also translates similarly

$$\Pr_{\epsilon}[h(\mathbf{x} + \epsilon) = 1] = \Pr_{\epsilon}[1 - h'(\mathbf{x} + \epsilon) = 1] = 1 - \Pr_{\epsilon}[h'(\mathbf{x} + \epsilon) = 1] = 1 - p$$

And the new problem is by definition same as  $1 - c^\downarrow[1 - p, \mathcal{B}]$   $\square$

**Lemma 3.** *If for a smoothing scheme, and a perturbation ball  $\mathcal{B}$ , canonical points can be used interchangeably; i.e. the solution to  $c^\uparrow$ , and  $c^\downarrow$  can be obtained on either of pairs  $(\mathbf{x}, \tilde{\mathbf{x}})$ , or  $(\tilde{\mathbf{x}}, \mathbf{x})$ , then we have  $c^\uparrow[c^\downarrow[p], \mathcal{B}], \mathcal{B}] = p$ .*

*Proof.* The term  $c^\uparrow[c^\downarrow[p], \mathcal{B}], \mathcal{B}]$  is expressed as the following optimization problem:

$$\begin{aligned} \max_{h \in \mathcal{H}} \Pr_\epsilon[h(\tilde{\mathbf{x}} + \epsilon) = 1] \quad \text{s.t.} \quad & \Pr_\epsilon[h(\mathbf{x} + \epsilon) = 1] = \min_{h' \in \mathcal{H}} \Pr_\epsilon[h'(\tilde{\mathbf{x}} + \epsilon) = 1] \\ \text{s.t.} \quad & \Pr_\epsilon[h'(\mathbf{x} + \epsilon) = 1] = \Pr_\epsilon[f(\mathbf{x} + \epsilon)] = p \end{aligned} \quad (6)$$

Note that (i) Both functions  $c^\uparrow$ , and  $c^\downarrow$  (and therefore both minimization and maximization) are non-decreasing to the value in their constraint. (ii)  $f$  is a feasible solution to both  $h$ , and  $h'$ . The later implies that  $c^\uparrow[c^\downarrow[p], \mathcal{B}], \mathcal{B}] \geq p$  as  $p$  is one of the feasible solutions. Now consider the specific solution resulting in probability  $p$ . Let  $p_l := \min_{h' \in \mathcal{H}} \Pr_\epsilon[h'(\tilde{\mathbf{x}} + \epsilon) = 1]$  on that specific configuration.

Now assuming that there exists a  $p^* > p$  as a solution for Eq. 6. Due to the non-decreasing property of the maximization problem, in the new configuration, we have  $p_l^+ := \min_{h' \in \mathcal{H}} \Pr_\epsilon[h'(\tilde{\mathbf{x}} + \epsilon) = 1] > p_l$ . Applying the same argument again we have  $\Pr_\epsilon[h'(\mathbf{x} + \epsilon) = 1] \neq p$  which contradicts the base constraint of the optimization. Therefore  $p$  is a feasible solution, and any solution higher than  $p$  is not feasible. A similar chain of arguments can be applied to show that  $c^\downarrow[c^\uparrow[p], \mathcal{B}], \mathcal{B}] = p$ .  $\square$

**Certified Upper and Lower bounds for all Shapes and Sizes.** Let  $g(\mathbf{x}) := \mathbb{E}_\epsilon[f(\mathbf{x} + \epsilon)]$  for any binary decision function  $f$  and any  $\epsilon \sim \xi$  where  $\xi(\mathbf{x}) \propto \exp(-\psi(\mathbf{x}))$ . If  $g(\cdot)$  is continuous in  $\mathcal{X}$ , for any point  $\tilde{\mathbf{x}} = \mathbf{x} + \delta$  one can compute the  $g(\mathbf{x} + \delta)$  through line integral as

$$g(\tilde{\mathbf{x}}) = g(\mathbf{x}) + \int_0^r \frac{d}{dt} [g(\mathbf{x} + t \cdot \delta)] dt$$

for  $\delta$  to be the unit vector in the same direction as  $\tilde{\delta}$  and  $r := \|\tilde{\delta}\|$ . In other words, we increment all the infinitesimal changes on the path from  $\mathbf{x}$  to  $\tilde{\mathbf{x}}$  to compute the value of  $g(\tilde{\mathbf{x}})$  given  $g(\mathbf{x})$ .

With the decision boundary  $\mathcal{U} = \{\mathbf{x} : f(\mathbf{x}) = 1\}$ , and  $\mathcal{U} - \mathbf{z}$  as the decision boundary translated from  $\mathbf{z}$  to the origin. Consider the following function

$$\Omega(\beta) := \sup_{\delta: \|\delta\|=1} \sup_{\mathcal{U} \in \mathbb{R}^d: \xi(\mathcal{U})=\beta} \lim_{r \rightarrow 0^+} \frac{\xi(\mathcal{U} - r\delta) - \beta}{r}$$

Proposition F.8 from Yang et al. [22] show that anywhere in  $\mathcal{X}$ , we have  $\frac{d}{dt} [g(\mathbf{z})] \leq \Omega(g(\mathbf{z}))$ . This means that one can upper bound the growth of  $g(\mathbf{x})$  while shifted by  $\delta$  by integrating over  $\Omega(g(\mathbf{z}))$  instead. For easier notation let  $h(t) = g(\mathbf{x} + t \cdot \delta)$  which implies  $h'(t) = \frac{d}{dt} h(t) \leq \Omega(h(t))$ . Notably the function  $\Omega(p)$  is always non-negative. We refer to Definition H.12 from Yang et al. [22] (originally the function is noted as  $\Phi(p)$ ) which is an expectation of a maximum over a value that is always non-negative ( $p$ , a quantile, or a random variable above that quantile). For positive (non zero)  $\Omega(h(t))$ , including but not limited to  $\beta \leq 1/2$  (see the definition of the function in Appendix F from Yang et al. [22]) It follows:

$$\frac{h'(t)}{\Omega(h(t))} \leq 1 \Rightarrow \int_0^r \frac{h'(t)}{\Omega(h(t))} dt \leq \int_0^r 1 dt = r$$

We set  $u = h(t) \Rightarrow du = h'(t)dt$  which implies

$$\Pi(u) = \int_0^r \frac{h'(t)}{\Omega(h(t))} dt = \int_{u=h(0)}^{u=h(r)} \frac{1}{\Omega(u)} du \leq r$$

The authors already computed  $\Omega(p)$  (in their paper it is called as  $\Phi$ ) for following several distributions, including:

- Isotropic Gaussian smoothing against  $\ell_2$  ball ( $\sigma = 1$ ):  $\Omega(u) = \Phi'(\Phi^{-1}(1 - u))$  which implies:

$$\Pi_{\text{Gaussian}}(u) = \int_{\beta}^{\bar{\beta}} \frac{1}{\Omega(u)} du = \int_{\beta}^{\bar{\beta}} \frac{1}{\Phi'(\Phi^{-1}(1 - u))} du$$

With  $c = \Phi^{-1}(1 - u)$  we have  $dp = -\Phi'(c)dc$ , and  $\Phi'(c) = \Phi'(\Phi^{-1}(1 - u))$ . Therefore

$$\begin{aligned} \int_{\beta}^{\bar{\beta}} \frac{1}{\Phi'(\Phi^{-1}(1 - u))} du &= \int_{\Phi^{-1}(1 - \beta)}^{\Phi^{-1}(1 - \bar{\beta})} -du = \Phi^{-1}(1 - \beta) - \Phi^{-1}(1 - \bar{\beta}) \leq r \\ \Rightarrow \Phi^{-1}(1 - \bar{\beta}) &\geq \Phi^{-1}(1 - \beta) - r \Rightarrow 1 - \Phi^{-1}(\bar{\beta}) \geq 1 - \Phi^{-1}(\beta) - r \\ &\Rightarrow \Phi^{-1}(\bar{\beta}) \leq \Phi^{-1}(\beta) + r \rightarrow \bar{\beta} \leq \Phi(\Phi^{-1}(\beta) + r) \end{aligned}$$

Which completely aligns with the aforementioned closed form  $\ell_2$  certificate.

- Laplace smoothing against  $\ell_1$  ball ( $\sigma = \sqrt{2}\lambda$ ):  $\Omega(u) = \frac{u}{\lambda}$  which implies:

$$\begin{aligned} \Pi_{\text{Laplace}}(u) &= \int_{\beta}^{\bar{\beta}} \frac{1}{\Omega(u)} du = \int_{\beta}^{\bar{\beta}} \lambda \frac{1}{u} du = \lambda \log \frac{\bar{\beta}}{\beta} \leq r \\ &\Rightarrow \frac{\bar{\beta}}{\beta} \leq 2^{r/\lambda} \Rightarrow \bar{\beta} \leq 2^{r/\lambda} \cdot \beta \end{aligned}$$

Note that in both cases, the function  $\Omega(p)$  is positive in  $(0, 1)$ .

Another easy way to obtain an upper bound is to use the robust radius (the closed form solution for  $\int_{\beta}^{1/2} \frac{1}{\Omega(p)} dp$ ) as a proxy. We have  $\int_{\beta}^{\bar{\beta}} \frac{1}{\Omega(p)} dp = \int_{\beta}^{1/2} \frac{1}{\Omega(p)} dp - \int_{\bar{\beta}}^{1/2} \frac{1}{\Omega(p)} dp$ . This function is monotonically increasing in  $[0, 1/2]$ , which means that we can use binary search to find the upper bound  $\bar{\beta}$  as:

$$\bar{\beta} = \sup \left\{ \hat{\beta} \in [\beta, 0.5] : \int_{\hat{\beta}}^{1/2} \frac{1}{\Omega(p)} dp \geq \int_{\beta}^{1/2} \frac{1}{\Omega(p)} dp - r \right\} \quad (7)$$

### D.3 RCP1: RCP1 Algorithm

Here we provide the pseudocode for RCP1. The algorithm is same as the conventional conformal prediction, with two specific difference. Instead of running a forward pass on the clean input, and then computing the conformity scores, we compute the forward pass over the noise augmented input. Note that despite other smoothing-based RCPs, here we only run one forward pass per each input. The other difference is that instead of the  $1 - \alpha$  coverage, we tune for the  $1 - \alpha'$  coverage taken from  $c^\uparrow$  function as discussed in § 3 (Eq. 4). Note that here there are no limitations on the score function and the model.

---

#### Algorithm 1: RCP1: Single Sample Robust Conformal Prediction

---

**Input:** Calibration set  $\mathcal{D}_{\text{cal}} = \{(\mathbf{x}_i, y_i)\}_{i=1}^n$ , score function  $s : \mathcal{X} \times \mathcal{Y} \rightarrow \mathbb{R}$ , test input  $\mathbf{x}_{n+1}$ , target coverage level  $1 - \alpha$ , perturbation ball  $\mathcal{B}_r$ , and smoothing scheme  $\xi$ .

**Output:** Prediction set  $\mathcal{C}_r(\mathbf{x}_{n+1}) \subseteq \mathcal{Y}$

---

- 1 **Step 1.** Draw noise from the smoothing scheme, compute conformity scores for augmented calibration data:
  - 2 **for**  $i = 1$  **to**  $n$  **do**
  - 3    $s_i \leftarrow s(\mathbf{x}_i + \epsilon_i, y_i)$  for  $\epsilon_i \sim \xi$
  - 4 **Step 2.** Compute  $1 - \alpha' = c^\uparrow[1 - \alpha, \mathcal{B}_r]$  from Eq. 4.
  - 5 **Step 2.** Compute the  $(1 - \alpha')$  quantile with correction:
  - 6  $q \leftarrow \mathbb{Q}(\alpha; \{s_1, \dots, s_n\})$  empirical quantile.
  - 7 **Step 3.** Construct the prediction set for the test input:
  - 8  $\mathcal{C}_r(\mathbf{x}_{n+1}) \leftarrow \{y \in \mathcal{Y} : s(\mathbf{x}_{n+1} + \epsilon_{n+1}, y) \geq q\}$
  - 9 **return**  $\mathcal{C}_r(\mathbf{x}_{n+1})$
- 

## E Supplementary Experiments

**Compute resources.** We ran our experiment using Nvidia A-100 and H-100 Tensor Core GPUs. For each experiment only one GPU was used. We use the A-100 GPU for the CIFAR-10 dataset under

Table 4: Empirical coverage and average set size for different radii ( $r$ ), for CIFAR-10 dataset with ResNet model and  $\sigma = 0.25$ .

$r$	Empirical Coverage	Avg Set Size
0.06	$0.936 \pm 0.018$	$2.156 \pm 0.241$
0.12	$0.961 \pm 0.014$	$2.646 \pm 0.306$
0.18	$0.981 \pm 0.010$	$3.315 \pm 0.478$
0.25	$0.990 \pm 0.008$	$4.178 \pm 0.798$
0.37	$1.000 \pm 0.000$	$10.000 \pm 0.000$
0.50	$1.000 \pm 0.000$	$10.000 \pm 0.000$
0.75	$1.000 \pm 0.000$	$10.000 \pm 0.000$

Table 5: Empirical coverage and average set size for different radii ( $r$ ), for CIFAR-10 dataset with ResNet model and  $\sigma = 0.5$ .

$r$	Empirical Coverage	Avg Set Size
0.06	$0.921 \pm 0.020$	$2.684 \pm 0.244$
0.12	$0.937 \pm 0.018$	$2.937 \pm 0.285$
0.18	$0.951 \pm 0.016$	$3.236 \pm 0.356$
0.25	$0.966 \pm 0.014$	$3.741 \pm 0.530$
0.37	$0.980 \pm 0.010$	$4.500 \pm 0.560$
0.50	$0.990 \pm 0.007$	$5.300 \pm 0.712$
0.75	$1.000 \pm 0.000$	$10.000 \pm 0.000$

ResNet setup, and the conformal risk control experiment. The rest of the results use H-100 as the compute resource.

**Experimental setup.** For the CIFAR-10 datasets we evaluate the results over 2048 test samples for ResNet model and 10000 images for the ViT models. For the ImageNet since the number of classes are 1000, we report our results over 5000 images for ViT models and 50000 images on ResNet models. Ultimately the number of samples does not influence the empirical results. The number of Monte Carlo samples are initially set to 500 for CIFAR and 300 for ImageNet. For each experiment, and for the reported sample rate we cut the precomputed samples, from the reported number.

Our results are reports over 100 runs (except the conformal risk control which is over one run. In each run we sample the 10% of the points as the calibration set. For conformal risk control we report the result on 300 images where 100 random images from it is taken for the calibration. Ultimately the size of the calibration set does not effect the final performance. As the calibration set gets larger the distribution of the coverage probability concentrates around  $1 - \alpha$ .

Noteworthy that in all cases, unless specified we set the nominal coverage to  $1 - \alpha = 0.9$ . Specifically for Fig. 5 we set this number to 90 and 95 (left and middle subplots) just to be able to compare with the reported numbers from Jeary et al. [14], and Massena et al. [17].

The time to compute the logits for the CIFAR-10 dataset is 1:30:56 (ViT with 10000 datapoints and 500 samples), and for the ImageNet dataset it is 13:52:11 (ViT with 5000 datapoints and 300 MC samples). For the ImageNet, and the ResNet model this number is 2:52:11 (for 50000 datapoints and 1000 samples).

**Set size experiment.** Tables Table 4 and Table 5 report the empirical coverage and average prediction set size of RCP1 for different radii  $r$  on the CIFAR-10 dataset using a ResNet model under two noise levels,  $\sigma = 0.25$  and  $\sigma = 0.5$ , respectively. We also report the result of the ImageNet dataset (for the ResNet model) in Table 6. Specifically for this dataset, because of the large number of classes we also reported the proportion of the sets below specific sizes (1, 3, 5, and 10). As expected, increasing the radius  $r$  results in a more conservative setup and hence higher coverage on the clean points. For CIFAR-10 dataset Fig. 10, and for the ImageNet dataset Fig. 11 visualize the comparative performance between BinCP and RCP1 across various radii and sampling budgets. These results are on the ResNet model. The heatmaps show the difference in set sizes  $|\mathcal{C}_{r,\text{BinCP}}| - |\mathcal{C}_{r,\text{RCP1}}|$ , where positive (green) values indicate that RCP1 provides smaller or more efficient sets. RCP1 generally outperforms BinCP across low sample rates, especially for smaller radii and moderate sampling budgets. The reference tables (Tables Table 4 and Table 5, Table 6) can be used to interpret these differences in absolute terms.

**Proportion of small sets.** As also discussed in § 4 although the proportion of sets with size less than a threshold shows how applicable a CP algorithm is, it can be misleading – a CP framework can return many false prediction sets with very small set size. Therefore alongside the proportion of these sets we should also report their coverage. We show these results in Fig. 12. Our observation is that all setups result in sets with coverage higher than the determined level. Note that in terms of proportion RCP1 stands somewhere between BinCP with 64 and 128 samples which aligns with our aforementioned intuition.

Table 6: Statistics from RCP1 across various radii. The results are for ImageNet dataset and the ResNet model.

$r$	Avg Set Size	Emp. Coverage	$\mathcal{C} \leq 1$	$\mathcal{C} \leq 3$	$\mathcal{C} \leq 5$	$\mathcal{C} \leq 10$
0.06	14.013 $\pm$ 1.787	0.921 $\pm$ 0.008	0.139 $\pm$ 0.010	0.311 $\pm$ 0.018	0.430 $\pm$ 0.025	0.626 $\pm$ 0.035
0.12	18.246 $\pm$ 2.606	0.936 $\pm$ 0.009	0.120 $\pm$ 0.010	0.274 $\pm$ 0.019	0.383 $\pm$ 0.024	0.560 $\pm$ 0.032
0.18	24.095 $\pm$ 3.645	0.951 $\pm$ 0.008	0.101 $\pm$ 0.010	0.239 $\pm$ 0.018	0.336 $\pm$ 0.023	0.501 $\pm$ 0.031
0.25	33.953 $\pm$ 5.744	0.964 $\pm$ 0.007	0.082 $\pm$ 0.008	0.201 $\pm$ 0.017	0.288 $\pm$ 0.022	0.432 $\pm$ 0.033
0.37	57.802 $\pm$ 10.753	0.979 $\pm$ 0.005	0.058 $\pm$ 0.008	0.151 $\pm$ 0.017	0.219 $\pm$ 0.022	0.337 $\pm$ 0.031
0.50	98.464 $\pm$ 19.136	0.989 $\pm$ 0.003	0.036 $\pm$ 0.006	0.104 $\pm$ 0.016	0.160 $\pm$ 0.021	0.252 $\pm$ 0.029
0.75	275.222 $\pm$ 88.968	0.998 $\pm$ 0.002	0.012 $\pm$ 0.006	0.036 $\pm$ 0.016	0.063 $\pm$ 0.025	0.115 $\pm$ 0.039
1.00	1000.000 $\pm$ 0.000	1.000 $\pm$ 0.000	0.000 $\pm$ 0.000	0.000 $\pm$ 0.000	0.000 $\pm$ 0.000	0.000 $\pm$ 0.000

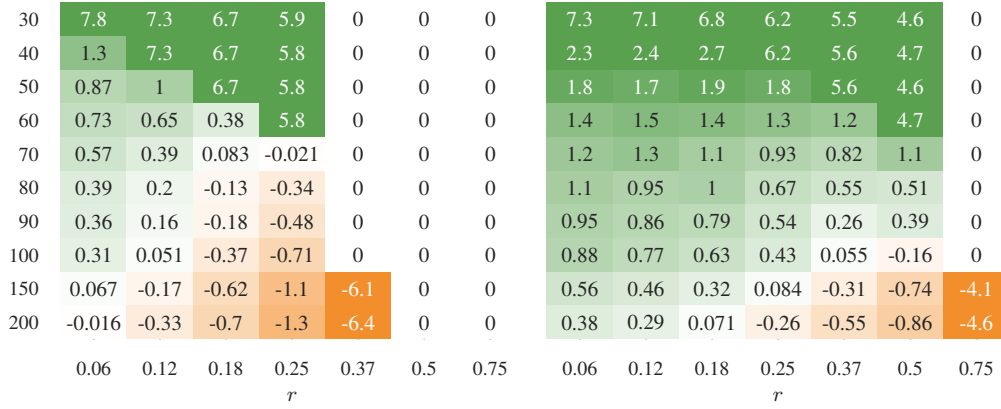


Figure 10: Comparison of BinCP and RCP1 in terms of  $|\mathcal{C}_{r,\text{BinCP}}| - |\mathcal{C}_{r,\text{RCP1}}|$  (higher (green) shows better performance for RCP1) across various radii and sample rates. Results are on the ResNet model and for the CIFAR-10 dataset. [Left]  $\sigma = 0.25$ , and [Right]  $\sigma = 0.5$ . Note that the numbers are in terms of difference and to compute the absolute number Table 4, and Table 5 can be used as reference.

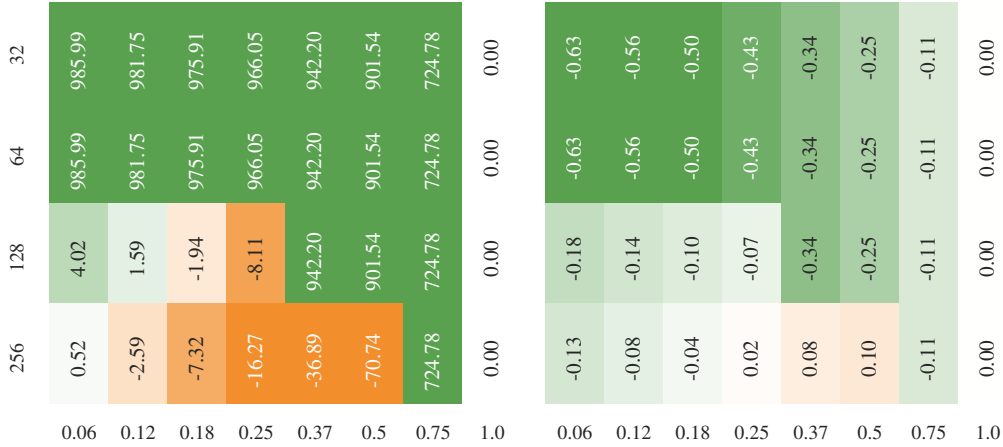


Figure 11: [Left] Comparison of the average set size  $|\mathcal{C}_{r,\text{BinCP}}| - |\mathcal{C}_{r,\text{RCP1}}|$  and [Right] the proportion of the sets with size  $\leq 10$  expressed in BinCP - RCP1. In both plots green shows that RCP1 is performing better. To convert the relative difference to absolute number Table 6 can be used as reference.

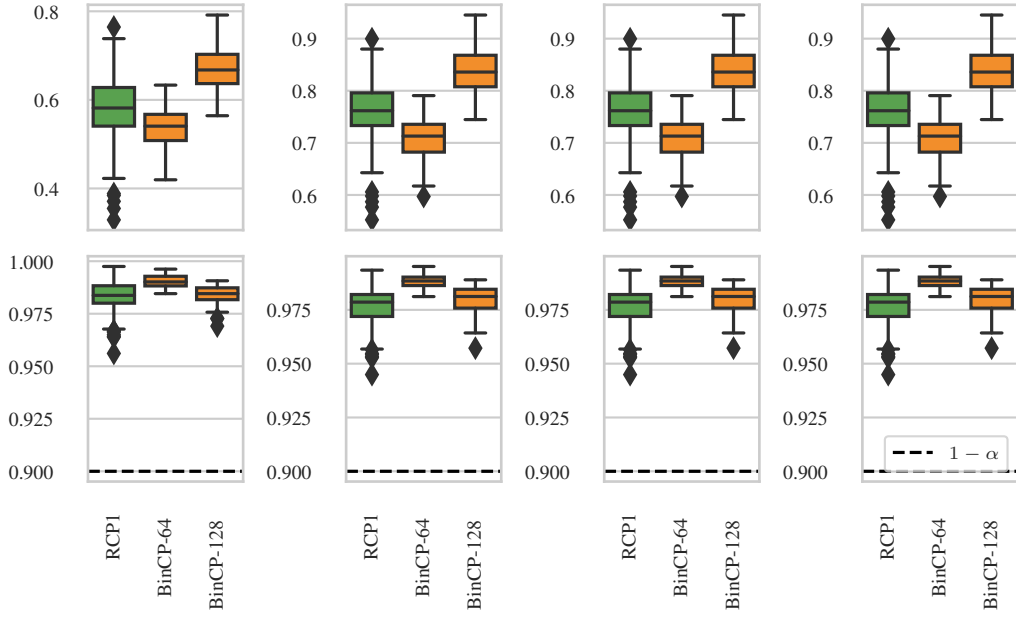


Figure 12: [Up] The proportion and [Bottom] the coverage of the prediction sets with size [From left to right]  $|\mathcal{C}| \leq 1$ ,  $|\mathcal{C}| \leq 3$ ,  $|\mathcal{C}| \leq 5$ ,  $|\mathcal{C}| \leq 10$ .